

How hydrophobic drying forces impact the kinetics of molecular recognition

Jagannath Mondal, Joseph A. Morrone, and B. J. Berne¹

Department of Chemistry, Columbia University, New York, NY 10027

Contributed by B. J. Berne, July 2, 2013 (sent for review May 30, 2013)

A model of protein–ligand binding kinetics, in which slow solvent dynamics results from hydrophobic drying transitions, is investigated. Molecular dynamics simulations show that solvent in the receptor pocket can fluctuate between wet and dry states with lifetimes in each state that are long enough for the extraction of a separable potential of mean force and wet-to-dry transitions. We present a diffusive surface hopping model that is represented by a 2D Markovian master equation. One dimension is the standard reaction coordinate, the ligand–pocket separation, and the other is the solvent state in the region between ligand and binding pocket which specifies whether it is wet or dry. In our model, the ligand diffuses on a dynamic free-energy surface which undergoes kinetic transitions between the wet and dry states. The model yields good agreement with results from explicit solvent molecular dynamics simulation and an improved description of the kinetics of hydrophobic assembly. Furthermore, it is consistent with a “non-Markovian Brownian theory” for the ligand–pocket separation coordinate alone.

hydrophobicity | hydrodynamics | non-Markovian effects | dewetting transitions

Recent theoretical work has shown that the displacement of water by drug molecules is important in the thermodynamics and kinetics of ligand–enzyme binding (1–3). The kinetics of drug docking is a key metric for lead optimization (4). Presently, we explore the kinetic motifs of hydrophobic association on ligand binding. This is achieved by developing a simple model for hydrophobic association that is compared with explicit solvent molecular dynamics (MD) simulation.

One of the signature features of hydrophobic assembly is the observation of a dewetting transition (5–9). Drying plays an important role in protein self-assembly and the behavior of nanoconfined water (10, 11). The present paper draws on our extensive work on the role of molecular-scale hydrodynamics in hydrophobic collapse (12, 13), where we showed that when the attraction between water and two associating nanoscale objects is weak, assembly proceeds via a drying transition in the intersolute region. This transition is characterized by large peaks in the relative translational friction coefficient that correspond to large and slow solvent fluctuations. The slow relaxation times exhibited by water undergoing dewetting transitions suggest that non-Markovian effects may prove to be a crucial element in a full description of the assembly kinetics.

We presently extend our earlier investigations to a model of a spherical ligand docking in a concave cavity. The model is similar to one investigated in a series of papers by McCammon and coworkers (14, 15), but is altered to describe the assembly of a nanoscale ligand. This alteration facilitates the study of a large-scale drying transition. We investigate molecular-scale hydrodynamic effects and the rate constants for binding and develop a theoretical framework to describe hydrophobic assembly. This theory couples the diffusive reaction coordinate (the separation) to transitions between “wet” and “dry” states which are defined by a coarse-grained solvent binding pocket occupancy. This model is conceptually similar to the surface hopping algorithm used in nonadiabatic quantum dynamics (16), and thus we call it the diffusive surface hopping model (DSHM). We show how the model reproduces the effect of drying fluctuations that are

evidenced in an ensemble of explicit solvent MD assembly trajectories.

In very recent work, Setny et al. (17) have computed the hydrodynamic profile for the ligand binding model that originated in ref. 14. It was found that enhanced and slowed hydration fluctuations engender a slowdown in the ligand dynamics, in agreement with our results on model plates and spheres (12, 13). This work also reported a shift in the spatial hydrodynamic effect that was attributed to non-Markovian effects. We find a related behavior in our study and show that it is resolved by use of the DSHM. In this way, the theoretical framework that is presently introduced yields a coarse-grained dynamical scheme that improves upon the description obtained from Smoluchowski (Brownian) dynamics when slow solvent motions are important.

Coarse-Grained Descriptions of Hydrophobic Assembly

Ligand binding kinetics is often described by the Smoluchowski equation:

$$\frac{\partial p(q, t)}{\partial t} = \frac{\partial}{\partial q} D(q) \left(\frac{\partial}{\partial q} - \beta \bar{F}(q) \right) p(q, t), \quad [1]$$

where q is the separation between ligand and receptor, $p(q, t)$ is the time-dependent probability distribution function, $\bar{F}(q) = -\partial W(q)/\partial q$ is the mean force, $W(q)$ is the potential of mean force, $D(q) = k_b T / \zeta(q)$ is the spatially dependent diffusion coefficient, and $\zeta(q)$ is the friction coefficient. This is a Markovian equation and is valid if solvent fluctuations are very fast compared with solute motions. The spatial dependence of the diffusion coefficient arises from hydrodynamic interactions (HI) between the receptor and ligand. $\bar{F}(q)$ and $\zeta(q)$ may be computed from MD (12, 13). Eq. 1 was tested in our previous work but we observed very slow solvent fluctuations at and around the drying transition between hydrophobic bodies. Indeed, the autocorrelation function of the solvent force along q exhibited prominent long time tails, indicating that non-Markovian effects should be important. In such cases, solvent degrees of freedom must be included in describing hydrophobic assembly (10, 18). We now develop a theory that is applicable to the ligand–receptor model. It includes a coarse-grained description of the solvent as an explicit degree of freedom of the dynamics, and involves a 2D Smoluchowski equation which, although Markovian, yields a non-Markovian expression for $p(q, t)$ in place of Eq. 1 when the solvent degree of freedom is projected out.

We propose a 2D model where one coordinate is the diffusive coordinate q (the separation between receptor and ligand) and the other is a discrete state variable $s = w$ or d , indicating whether the binding pocket is wet or dry, respectively. This model has state-dependent diffusion coefficients, $D(w, q)$ and $D(d, q)$, evolves on state-dependent free-energy surfaces, $W(w, q)$ and $W(d, q)$,

Author contributions: J.M., J.A.M., and B.J.B. designed research, performed research, analyzed data, and wrote the paper.

The authors declare no conflict of interest.

¹To whom correspondence should be addressed. E-mail: bb8@columbia.edu.

This article contains supporting information online at www.pnas.org/lookup/suppl/doi:10.1073/pnas.1312529110/-DCSupplemental.

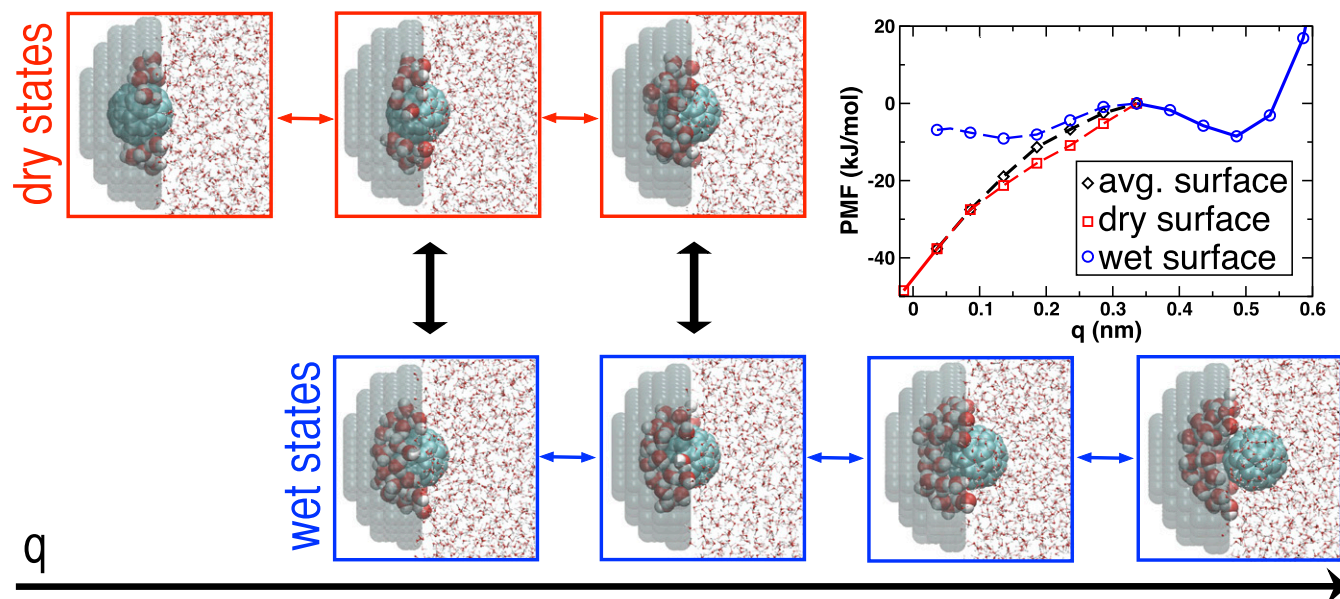


Fig. 1. Schematic for the Markovian master equation analysis that is presently used. Transitions among wet states (blue framed snapshots) and dry states (red framed snapshots) occur along q . Transitions between wet and dry states may occur in the dewetting region at fixed q . (Upper Right) Potential of mean force is plotted on the wet surface (blue line) and dry surface (red line). In the region of drying, two of the models presently considered evolve along a potential of mean force derived from the average of the mean forces for wet and dry states (black dashed line). Beyond $q=0.5$ nm, an external repulsive potential is added as described in the text. Snapshots are rendered with visual molecular dynamics (VMD) (33).

and its state can change from wet to dry and from dry to wet by first-order kinetics with rate constants also depending on q , namely $k(d \leftarrow w, q)$ and $k(w \leftarrow d, q)$ are the rate constants to transition from $w \rightarrow d$ and $d \rightarrow w$, respectively. This model is equivalent to a diffusing particle that can hop between two surfaces, one wet and one dry, with different spatially dependent diffusion constants on each surface. We call this the DSHM. Such a scheme can be described by the following differential equation for the time evolution of the probability density $p(s, q, t)$:

$$\frac{\partial p(s, q, t)}{\partial t} = \frac{\partial}{\partial q} D(s, q) \left(\frac{\partial}{\partial q} - \beta \bar{F}(s, q) \right) p(s, q, t) - k(s' \leftarrow s, q) p(s, q, t) + k(s \leftarrow s', q) p(s', q, t), \quad [2]$$

where $\bar{F}(s, q) = -\partial_q W(s, q)$. One equation, where $s=w$ and $s'=d$, is paired with one corresponding to $s=d$ and $s'=w$. In this way, the diffusion dynamics is coupled to transitions between the surfaces.

DSHM reduces to Eq. 1 when the hopping rate between surfaces is fast compared with the rate of diffusion along q (SI Text). This model is similar in spirit to one discussed in ref. 19 where diffusing charged particles in an electric field can hop between two states with different diffusion coefficients and electric mobilities, with the hopping governed by first-order kinetics. However, in this prior formulation the spatial dependence of the diffusion coefficients, electrical mobilities, and transition rates is ignored.

Application of Eq. 2 calls for specifying the mean force and diffusion coefficient separately for both the wet and dry states as well as a set of transition rates between these states. The problem can be simplified as transitions between wet and dry states only take place for separations in a narrow range. We assume that for large values of q only wet states are accessible and for small values of q only dry states are accessible. Then one need only consider transitions between surfaces in a specific “drying region.” One can then discretize the continuous Smoluchowski dynamics (20), and place both Eqs. 1 and 2 in the form of a Markovian master equation $\partial_t p_i(t) = R_{ij} p_j(t)$, where the index i

runs over all allowed states and where q is represented on a grid. The detailed expressions for R_{ij} in the case of both one dimensional Smoluchowski (Brownian) dynamics and our 2D two-surface representation are given in *Materials and Methods*, and a schematic depicting how transitions are made in a two-surface model is depicted in Fig. 1. Markovian master equations (Markov state models) can serve as an important tool to analyze conformational changes in biomolecules and extract kinetic information from molecular simulation (21), and have been also used to treat solvent degrees of freedom, including drying fluctuations in carbon nanotubes (22, 23).

The elements of the rate matrix are obtained from explicit solvent MD trajectories where the ligand–pocket separation is restrained to a set of values. The model ligand is a C60 fullerene and the pocket is an ellipsoidal hole carved from a hydrophobic slab. Further details are given in *Materials and Methods* and *SI Text*.

Results and Discussion

Average Mean Force and Hydrodynamic Profiles. The nature of the free-energy surface and hydrodynamic interactions that the solute experiences depends intrinsically on the strength of the solute–water interaction. Vastly different behavior is exhibited in the case of very hydrophobic bodies where assembly is facilitated by drying compared with more hydrophilic bodies where steric interactions engender the expulsion of water at small separations. We have computed the potential of mean force and hydrodynamic profile for the model pocket for three different strengths of solvent attraction. The interactions that describe the ligand are not varied. The weakest and intermediate interactions conform to the case of hydrophobic assembly driven by drying transitions, whereas the behavior of the strongly attractive pocket is dominated by steric ejections of water. The intermediate strength of attraction will be the focus of this work; discussion of the other two cases is presented in *SI Text*.

Fig. 2 B and D show how the number of water molecules in the first solvation shell of the ligand N_{Ligand} and the number of pocket water molecules N_{Pocket} vary as a function of the reaction coordinate q . As the (rather hydrophilic) ligand enters the pocket

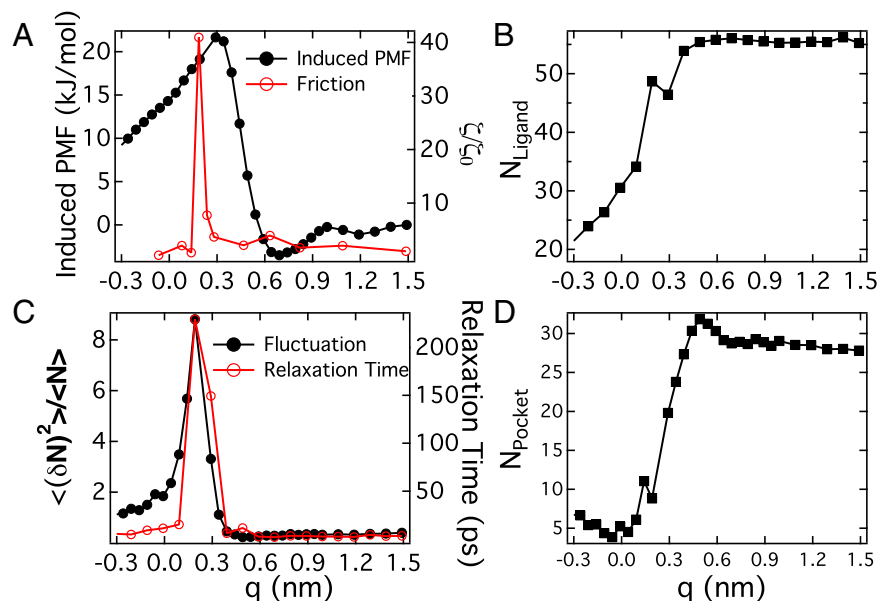


Fig. 2. Various thermodynamic and hydrodynamic profiles as a function of ligand-pocket separation for the intermediate-attractive pocket. (A) Comparison of the solvent-induced potential of mean force (left scale) and friction profile (right scale), (B) ligand-water number. (C) Correlation of pocket-water fluctuation (left scale) and relaxation time (right scale), and (D) pocket-water number.

there is a free-energy penalty associated with the stripping away of waters from the fullerene. There is also an observed maximum in the number of pocket-water molecules owing to the intrusion of the ligand solvation shell into the pocket. As the ligand further penetrates into the pocket, where the solvent-induced mean force is attractive, a drying transition centered at $q_c = 0.186$ nm occurs. The largest separation at which drying is observed corresponds to the top of the barrier ($q = 0.336$ nm).

The solvent-induced potential of mean force and variation of the friction coefficient with separation q are plotted in Fig. 2A. In prior work we computed the friction coefficient from the force autocorrelation function (24), whereas we presently use a technique that applies a harmonic restraint along the q direction at selected positions and probes the relaxation of the position autocorrelation function (25, 26). The region of drying is associated with a large peak in the friction coefficient, $\zeta(q)$ relative to its value at large separation, ζ_0 .

Plotted as a function of q in Fig. 2C are the solvent fluctuations and relaxation times in the binding pocket, the expressions for which are given in *SI Text*. These properties have been found to yield trends relatable to those observed for the profile of the friction coefficient in our previous work (12, 13), and this is also presently observed. It is seen that relaxation times greater than 200 ps are present in the cavity near the dewetting transition. As we will show later, this timescale is of the same order as the mean first passage time for the ligand to bind to the pocket starting from entry into the pocket. Such slow fluctuations indicate that the simple one-dimensional Brownian dynamics approximation does not hold, and non-Markovian effects are significant.

Hydrophobic Forces on Wet and Dry Surfaces. A detailed characterization of the underlying solvent coordinate in the DSHM calls for a quantitative analysis of the dry and wet states observed in the dewetting region. The probability distribution and representative trajectory of the pocket water molecules are shown for $q = q_c$ in Fig. 3A and B. From the plot of the number of waters in the region between ligand and pocket versus time in A, one sees that the wet and dry states have sufficiently long survival times, and therefore various average properties for the wet and dry states can be determined.

To underline the importance of the slow fluctuations between wet and dry states at the dewetting transition, we plot the normalized position autocorrelation function of the total system in Fig. 3D and for the wet and dry states separately in Fig. 3C. One

can see that the relaxation times of the correlation functions are markedly shorter when the states are considered separately. The friction coefficient in the wet and dry states may be estimated from the correlation function $\langle q(0)q(t) \rangle$ using the approach in refs. 25 and 26. The friction in the wet state is close to the value found at large separations, whereas in the dry state it is approximately half of this. Therefore, the pronounced hydrodynamic effect we observe at the drying transition in this and prior studies is shown to be due to slow transitions between the wet and dry states, and it is appealing to incorporate this as a separate slow collective variable, whereas other solvent degrees of freedom remain treatable in the Markovian limit. Indeed, this is the rationale behind the DSHM.

Constructing the DSHM. The parameterization of our DSHM draws from the underlying simulation results as obtained in the region of the drying transition. As evident from Eq. 2, the three main inputs necessary for DSHM are the mean force and diffusion coefficient along the two surfaces and the rate constants for transitions between wet and dry states. Here, we will briefly outline only the salient features of how we construct the DSHM using simulation as the source of parameters. A detailed discussion of the parameterization is reserved for *SI Text*.

The DSHM requires mean forces on the dry and wet surfaces. It consists of numerous wet and dry states set on an equally spaced grid along q . For the purpose of this model, a state is defined as dry if there are fewer than 15 water molecules in the pocket, and wet otherwise. We extract mean dry and wet forces by averaging over wet and dry configurations separately at each fixed q in the dewetting region. The resulting potentials of mean forces, which include the direct interactions of heavy bodies that correspond to the wet and dry surfaces, are plotted in Fig. 1.

Another crucial set of input parameters for DSHM are the rate constants for the transitions, wet \rightleftharpoons dry. Such transitions are only treated in the dewetting region. Only wet and dry states are considered at large and small separations, respectively. The matrix elements are estimated from the average dwell times in the wet state from MD simulations at fixed q . The reverse transitions are then estimated from the detailed balance condition and the equilibrium probabilities of being in a wet or dry state. The values of the inverse rate constants at the values of q considered are given in Table 1. The transition times are shown to become shorter as the bodies approach each other and fewer water molecules are displaced by the drying event. Recent work on the rate of drying

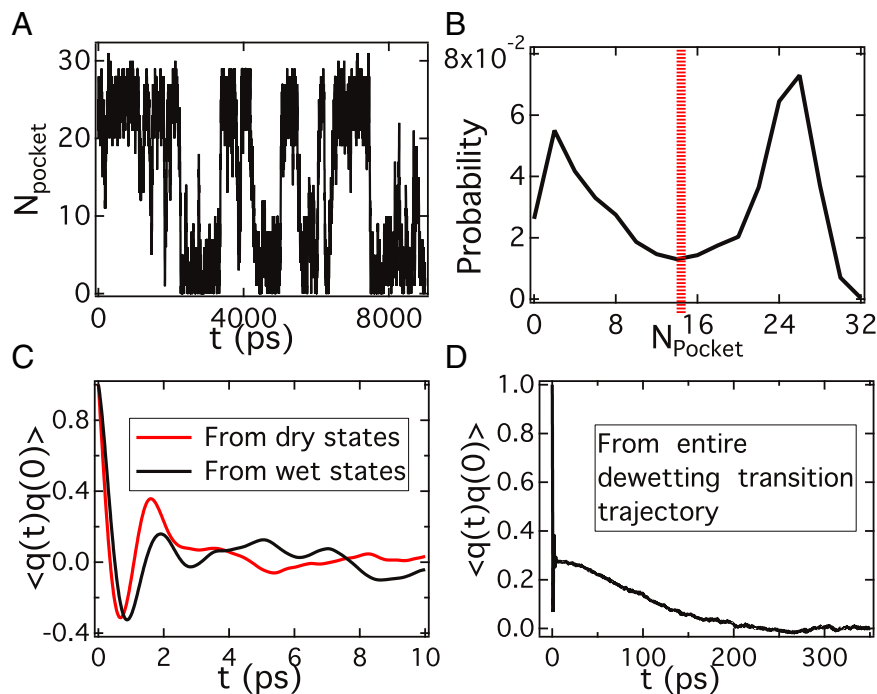


Fig. 3. (A) Representative trajectory exhibiting fluctuations between wet and dry states at $q_c = 0.186$ nm. (B) Probability distribution of solvent occupancy in the pocket at q_c . Configurations to the left and right of the dashed red line are considered to be dry or wet, respectively. The normalized position autocorrelation function about $\langle q \rangle = q_c$ is plotted in the wet (black line) and dry (red line) states in C and the total autocorrelation function from which the friction coefficient at q_c is determined is plotted in D. The long tail of the total correlation function is absent in the wet and dry state results, indicating that the large friction is associated with slow solvent fluctuations due to drying and wetting events.

(8, 9) finds that the activation free energy depends on distance through linear and quadratic terms which are related through macroscopic arguments to surface and line tensions. We find our present data set too sparse to elaborate on this finding. At small separations, we include two states on the wet surface for which the solvation state is dry for long times. The inclusion of such “transient wet” states, which may be visited as the ligand diffuses along q , places the kinetics of assembly predicted by the model in quantitative agreement with molecular dynamics simulation.

The diffusion coefficient in the dewetting region is taken to be constant, albeit with different values on the wet and dry surfaces ($D_{\text{wet}} = D_{\text{dry}}/2 = 7.56 \times 10^{-4}$ nm²/ps). This ratio is estimated from the data presented in Fig. 3C and also by considering the hydrodynamic profile at small separations (Fig. 2A). The value of D_{wet} is taken to be the diffusion constant for the ligand at large separations. In this way, the hydrodynamic effect in the dewetting region is subsumed into the wet-to-dry transitions which are an explicit degree of freedom of the dynamics given by Eq. 2. Outside this region, D is parameterized from the frictional profile (Fig. 2A).

Comparison of DSHM with Other Dynamical Schemes. To directly compare the dynamics of the DSHM to explicit solvent MD simulation and to one-dimensional Smoluchowski dynamics, we determine the time-dependent spatial distribution function $P(q, t)$ and the mean first passage times (MFPTs) for assembly from MD simulations where the pocket is fixed and the ligand is free to move

Table 1. Period of wet to dry transitions and equilibrium occupancy of wet and dry states

q , nm	$k^{-1}(q, d \leftarrow w)$, ps	P_{dry}	P_{wet}
0.036	6.0	—	—
0.086	20.0	—	—
0.136	75.8	0.74	0.26
0.186	193	0.44	0.56
0.236	212	0.29	0.71
0.286	276	0.38	0.62
0.336	519	0.17	0.83

At small q , no occupancy is given as it is dominated by the dry state.

in the direction of q . To guarantee that the ligand cannot diffuse far from the binding site, a repulsive wall potential is added to the system. The resultant potential of mean force, including the repulsive wall, is depicted in Fig. 1. Note that these simulations differ from those from which the model parameters were determined, where q was fixed at different values.

Apart from comparing with MD simulations, it is also of interest to compare the 2D model (DSHM) to one-dimensional diffusion (Smoluchowski) dynamics on the average potential of mean force described by the Markovian master equation including either a position-dependent or a constant diffusion coefficient (20). The diffusive dynamics occurs on the average potential of mean force that includes contributions from both wet and dry states. In the Avg-HI model, hydrodynamic interactions are described by the friction coefficient profiles depicted in Fig. 2A. In the case of no hydrodynamic interaction (Avg-NOHI), the diffusion constant D_{wet} is used for all values of q .

The spatial probability distribution at time t , $p(q, t) = \sum_s p(s, q, t)$, can be compiled from a set of MD trajectories and compared with the results for the models that are obtained from solving the master equation. The probability distribution at $t = 50$ ps and $t = 100$ ps is plotted in Fig. 4. It can be readily seen that the MD result exhibits three peaks: one corresponding to the basin in the mean force that is created by the wall potential at large separations, a smaller, more transient peak in the dewetting region, and a peak corresponding to ligand in the docked pose. For long times, the distribution is localized in the docked pose, or in the case of master equation models, in the absorbing state.

Whereas all master equation models considered reproduce the features at the ligand far from the pocket and for the ligand in the docked pose, the peak resulting from drying fluctuations is not described by the average potential of mean force alone (which is strictly attractive in this region). The results for MD and the DSHM are in good agreement in this region (Fig. 4, *Insets*), as the model captures the peak position and decay from $t = 50$ ps to $t = 100$ ps very well given the model’s resolution.

The results for Avg-HI given in Fig. 4 also exhibit a peak in $p(t)$ in the drying region, but it is shifted with respect to the results of the MD and the DSHM. This peak is shifted to the right of where the friction coefficient peaks and is related to where the

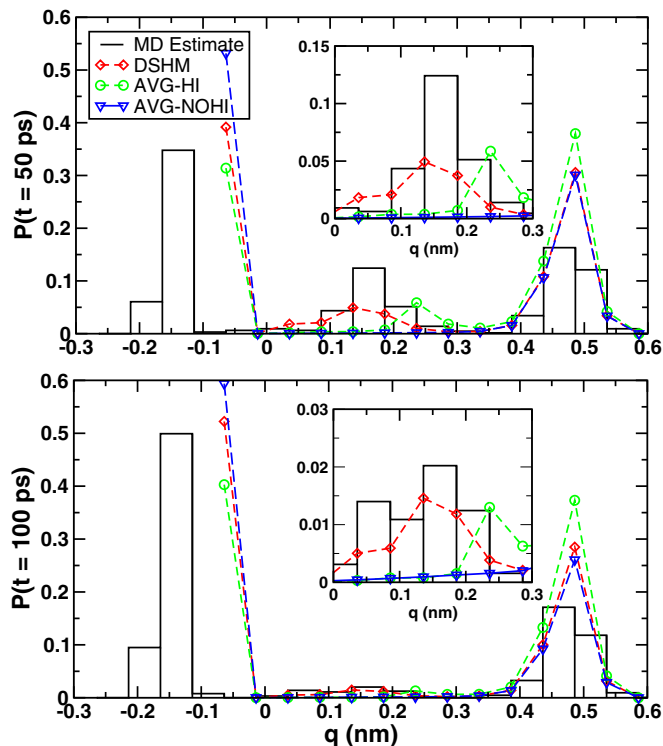


Fig. 4. Probability distribution of the assembly process at $t=50$ ps (Upper) and $t=100$ ps (Lower). Results from MD simulation (black bars) are compared against those extracted from theories that can be expressed as Markovian master equations, one where the distribution evolves on two surfaces (DSHM, red line with diamonds), and others where it evolves on an average surface with (Avg-HI) and without hydrodynamic interactions (Avg-NOHI) (green line with circles and blue line with triangles, respectively). (Insets) Distributions in the drying region.

smallest element of R_{ij} appears in the dewetting region (*Materials and Methods*). In the DSHM, the peak position is determined by the local minimum on the wet surface and agrees well with the MD result. This shift in peak position is reminiscent of that reported in ref. 17, where a difference was observed in the $\zeta(q)$ computed from simulations in which q is restrained, and an effective spatial friction extracted from MFPT data. The authors attributed this shift to non-Markovian effects which are well captured by DSHM.

The MFPTs for assembly initiated from a wet state at $q_0 = 0.336$ nm are given in Table 2 for the models considered. It can be seen that, among all dynamical schemes presently considered, the MFPT obtained from DSHM comes closest to the results obtained from MD. The Avg-HI result significantly overestimates the MFPT. On the other hand, the MFPT obtained from Avg-NOHI is a drastic underestimation of the result obtained from simulation, partly because it lacks a description of the drying transition.

To gain a more detailed understanding of the kinetics in the drying region, we compute the MFPT to assembly from initial wet configurations at pocket–ligand separations where the average

Table 2. MFPT as extracted from various models

Model	MFPT (ps)		MFPT (ps)
	$q_0 = 0.336$ nm	$q_0 = 0.286$ nm	$q_0 = 0.186$ nm
MD	473	44	42
DSHM	351	42	34
Avg-HI	816	52	5
Avg-NOHI	193	9	3

surface points downhill toward assembly. Trajectories (about 3%) that recross into the region beyond the drying transition are not counted for the purpose of this calculation. The DSHM is in agreement with the results obtained from MD. As expected, the Avg-NOHI MFPT is far too low owing to its lack of a description of the drying phenomena. Interestingly, the Avg-HI model yields a reasonable result for one initial condition ($q_0 = 0.286$ nm) but not the other ($q_0 = 0.186$ nm). This result is another manifestation of the spatial shift of the probability distribution discussed above, such that the large hydrodynamic slowdown does not influence the (Avg-HI) results when the ligand is initially placed to the left of the center peak in Fig. 4.

Conclusions

A full assessment of the kinetics of molecular recognition processes calls for the inclusion of molecular-scale hydrodynamic effects. However, most typically in coarse-grained models such effects are either ignored or treated within Markovian limit where the solvent timescales are assumed to be fast compared with those of the heavy bodies. In reality, however, slow solvent fluctuations are present when confined water molecules are expelled from the region between the ligand and the pocket wall. The non-Markovian nature of this problem begs for a more comprehensive theory which includes the solvent as an explicit part of the reaction path.

We present a simple model to study the kinetics of ligand binding in a model hydrophobic enclosure in conjunction with a coarse-grained theory in which solvent is accounted for by introducing a discrete state variable specifying whether the pocket is dry or wet. In this way, diffusive motion along the (heavy-body) assembly coordinate is coupled to transitions between the wet and dry surfaces. This model is found to yield an improved description of the assembly process compared with models that ignore these state changes and obey standard Smoluchowski (Brownian) dynamics. In this way, the leading phenomena that give rise to non-Markovian behavior may be subsumed into a Markovian master equation description that lies in a larger state space.

Here, we have explored the role of solvent in the kinetics of ligand–pocket association. Although our model is rather crude, it is still able to capture the displacement of water molecules by a ligand via hydrophobic drying transitions and the free-energy barrier associated with ligand desolvation. However, the ligand pocket is rather smooth and interactions are only mediated through the Lennard-Jones potential and not specific hydrogen bonding. Indeed, the presence of water may be more or less favorable near heterogeneous surfaces (27) or in different regions of the pocket (1). Furthermore, the pocket and the ligand are both rigid structures in the simulations and the coupling of ligand and pocket internal degrees of freedom is not presently considered. Such effects may be rather slow and essential in the pathway to

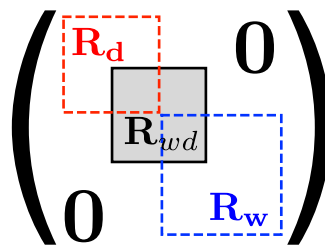


Fig. 5. Schematic of the addition of the matrices that comprise the rate matrix, R . Transitions along q on the dry surface are described by R_d , and along the wet surface by R_w . R_{wd} mediates transitions between the surfaces. The nonzero blocks of these matrices are denoted by the red, blue, and black boxes, respectively.

assembly, and may be incorporated in modified diffusive surface hopping models.

Assembly processes that occur in a bath of lighter particles are important in a wide variety of settings. MD simulations provide an excellent tool for the study of such systems, although a deep understanding can be gained from the relation of large-scale simulations to more coarse-grained models of diffusion on smaller subsets of collective variables. This understanding can further clarify the kinetics of assembly processes and be incorporated into coarse-grained models. Future work will address this relation, as well as the behavior of patchy, softer, and more realistic bodies.

Materials and Methods

Expression for Elements of Dynamic Matrix. The Markovian master equation description is given by the expression $\partial_t p_i(t) = R_{ij} p_j(t)$ for the evolution of the probability distribution in state i , $p_i(t)$. In the two-surface model, the index i runs over all allowed wet and dry states. The diffusive coordinate q is represented on a grid of spacing Δq . The matrix \mathbf{R} can be expressed as the sum of three matrices that describe distinct types of transitions,

$$\mathbf{R} = \mathbf{R}_d + \mathbf{R}_w + \mathbf{R}_{wd}. \quad [3]$$

A diagram of this addition is shown in Fig. 5. The total dimension of \mathbf{R} is $N_w + N_d$. The matrices \mathbf{R}_d and \mathbf{R}_w describe transitions along q in the dry and wet states, respectively, and have the following form:

$$R_s(q_i, q_j) = -[\omega_{+,j}^{(s)} + \omega_{-,j}^{(s)}] \delta_{ij} + \omega_{+,j}^{(s)} \delta_{i+1,j} + \omega_{-,j}^{(s)} \delta_{i-1,j}, \quad [4]$$

where “ s ” denotes either a wet or dry state,

$$\omega_{+,n}^{(s)} = \frac{D(s, q_{n+1}) + D(s, q_n)}{2\Delta q^2} \exp(+\alpha) \quad [5]$$

$$\omega_{-,n}^{(s)} = \frac{D(s, q_{n-1}) + D(s, q_n)}{2\Delta q^2} \exp(-\alpha), \quad [6]$$

where $\alpha = (\beta\Delta q/4)[\bar{F}(s, q_{n+1}) + \bar{F}(s, q_n)]$, and where D and \bar{F} are the diffusion coefficient and mean force on a particular surface, respectively. These expressions represent a discretization of the Smoluchowski equation (20).

In the Markovian (Brownian) limit, this expression along a single, averaged surface is considered. The spatial dependence in the diffusion coefficient engenders a maximum slowdown in the transition probability R_{ij} where the sum of the diffusion coefficients in states i and j is minimum. For the profile plotted in Fig. 2 this occurs at $q = 0.236$ nm, and is reflected in the peak position of $p(q, t)$ that is observed in the Avg-HI model (Fig. 4). The peak position also can depend on \bar{F} , but it is roughly constant in the dewetting region on the average surface.

In the range of separations where wet-to-dry transitions may occur, they are described by the matrix \mathbf{R}_{wd} . If N_{wd} is the number of values of q for which such transitions are allowed, then the matrix is (square) block diagonal where the block has dimension of $2N_{wd}$. This block has diagonal elements: $-k(q, w \leftarrow d)$ for indices less than or equal to N_{wd} and $-k(q, d \leftarrow w)$ for indices greater than N_{wd} . The off-diagonal components are nonzero for transitions between wet and dry states at the same value of q . The lifetime of the wet state is the inverse of the transition rates given in Table 1.

Simulation Details. The model system presently used is inspired by the one developed in ref. 14 but with some distinct features, most notably that the sizes of the ligand and the pocket are larger, with a length scale on the order of 1 nm. All simulations are performed in explicit TIP4P water (28) with the GROMACS MD package (29). During the equilibration stage, temperature and pressure are controlled with the stochastic velocity rescaling thermostat (30) and the barostat of Berendsen (31). The parameters of \mathbf{R} are extracted from MD simulations where the ligand–pocket separation q is restrained. The MFPT for assembly is computed from averaging over 645 trajectories where the pocket is fixed, but the ligand is free to move in the q direction. A repulsive wall is included to ensure that all configurations assemble and is explicitly accounted for in comparison with the master equation approaches. This is achieved with the PLUMED plugin for GROMACS (32). As the drying kinetics is sensitive to the chosen conditions, it is noted that all simulations were run at 300 K and 1 bar, typical of biological conditions. Further details of the model and protocol are given in *SI Text*.

ACKNOWLEDGMENTS. This work was supported by the National Institutes of Health (NIH-GM4330) and the National Science Foundation (NSF), NSF-CHE-0910943. We also acknowledge support from the Computational Center for Nanotechnology Innovations at Rensselaer Polytechnic Institute. This work used the Extreme Science and Engineering Discovery Environment, which is supported by the NSF (OCI-1053575).

- Young T, Abel R, Kim B, Berne BJ, Friesner RA (2007) Motifs for molecular recognition exploiting hydrophobic enclosure in protein-ligand binding. *Proc Natl Acad Sci USA* 104(3):808–813.
- Shan Y, et al. (2011) How does a drug molecule find its target binding site? *J Am Chem Soc* 133(24):9181–9183.
- Dror RO, et al. (2011) Pathway and mechanism of drug binding to G-protein-coupled receptors. *Proc Natl Acad Sci USA* 108(32):13118–13123.
- Copeland RA, Pompliano DL, Meek TD (2006) Drug-target residence time and its implications for lead optimization. *Nat Rev Drug Discov* 5(9):730–739.
- Berne BJ, Weeks JD, Zhou R (2009) Dewetting and hydrophobic interaction in physical and biological systems. *Annu Rev Phys Chem* 60:85–103.
- Rasaiah JC, Garde S, Hummer G (2008) Water in nonpolar confinement: From nanotubes to proteins and beyond. *Annu Rev Phys Chem* 59:713–740.
- Chandler D (2005) Interfaces and the driving force of hydrophobic assembly. *Nature* 437(7059):640–647.
- Sharma S, Debenedetti PG (2012) Evaporation rate of water in hydrophobic confinement. *Proc Natl Acad Sci USA* 109(12):4365–4370.
- Sharma S, Debenedetti PG (2012) Free energy barriers to evaporation of water in hydrophobic confinement. *J Phys Chem B* 116(44):13282–13289.
- Liu P, Huang X, Zhou R, Berne BJ (2005) Observation of a dewetting transition in the collapse of the melittin tetramer. *Nature* 437(7055):159–162.
- Hummer G, Rasaiah JC, Noworyta JP (2001) Water conduction through the hydrophobic channel of a carbon nanotube. *Nature* 414(6860):188–190.
- Morrone JA, Li J, Berne BJ (2012) Interplay between hydrodynamics and the free energy surface in the assembly of nanoscale hydrophobes. *J Phys Chem B* 116(11):378–389.
- Li J, Morrone JA, Berne BJ (2012) Are hydrodynamic interactions important in the kinetics of hydrophobic collapse? *J Phys Chem B* 116(37):11537–11544.
- Baron R, Setny P, McCammon JA (2010) Water in cavity-ligand recognition. *J Am Chem Soc* 132(34):12091–12097.
- Baron R, McCammon JA (2013) Molecular recognition and ligand association. *Annu Rev Phys Chem* 64:151–175.
- Tully JC (2012) Perspective: Nonadiabatic dynamics theory. *J Chem Phys* 137(21):22A301–1–22A301-7.
- Setny P, Baron R, Michael Kekenes-Huskey P, McCammon JA, Dzubiella J (2013) Solvent fluctuations in hydrophobic cavity-ligand binding kinetics. *Proc Natl Acad Sci USA* 110(4):1197–1202.
- Willard AP, Chandler D (2008) The role of solvent fluctuations in hydrophobic assembly. *J Phys Chem B* 112(19):6187–6192.
- Berne BJ, Pecora R (1990) *Dynamic Light Scattering: With Applications to Chemistry, Biology, and Physics* (Dover, New York).
- Bicout DJ, Szabo A (1998) Electron transfer reaction dynamics in non-Debye solvents. *J Chem Phys* 109(6):2325–2338.
- Pande VS, Beauchamp K, Bowman GR (2010) Everything you wanted to know about Markov State Models but were afraid to ask. *Methods* 52(1):99–105.
- Sriraman S, Kevrekidis IG, Hummer G (2005) Coarse master equation from Bayesian analysis of replica molecular dynamics simulations. *J Phys Chem B* 109(14):6479–6484.
- Gu C, et al. (2013) Building Markov state models with solvent dynamics. *BMC Bioinformatics* 14(Suppl 2):S8.
- Bocquet L, Hansen J, Piasecki J (1997) Friction tensor for a pair of Brownian particles: Spurious finite-size effects and molecular dynamics estimates. *J Stat Phys* 89(1-2):321–346.
- Straub JE, Berne BJ, Roux B (1990) Spatial dependence of time-dependent friction for pair diffusion in a simple fluid. *J Chem Phys* 93(9):6804–6812.
- Hummer G (2005) Position-dependent diffusion coefficients and free energies from Bayesian analysis of equilibrium and replica molecular dynamics simulations. *New J Phys* 7:34.
- Giovambattista N, Debenedetti PG, Rossky PJ (2007) Hydration behavior under confinement by nanoscale surfaces with patterned hydrophobicity and hydrophilicity. *J Phys Chem C* 111(3):1323–1332.
- Jorgensen W, Chandrasekhar J, Madura J, Impey R, Klein M (1983) Comparison of simple potential functions for simulating liquid water. *J Chem Phys* 79:926–935.
- Hess B, Kutzner C, van der Spoel D (2008) Gromacs 4: Algorithms for highly efficient, load-balanced, and scalable molecular simulation. *J Chem Theory Comput* 4(3):435–447.
- Bussi G, Donadio D, Parrinello M (2007) Canonical sampling through velocity rescaling. *J Chem Phys* 126(1):014101.
- Berendsen HJC, Postma JPM, van Gunsteren WF, DiNola A, Haak JR (1984) Molecular dynamics with coupling to an external bath. *J Chem Phys* 81(8):3684–3690.
- Bonomi M, et al. (2009) PLUMED: A portable plugin for free-energy calculations with molecular dynamics. *Comput Phys Commun* 180:1961–1972.
- Humphrey W, Dalke A, Schulten K (1996) VMD: Visual molecular dynamics. *J Mol Graph* 14(1):33–38, 27–28.